Compton-profile measurements for W, Ag, and Cu with 662-keV γ rays

Maria Vittoria Heller and José Roberto Moreira
Department of Experimental Physics, São Paulo University, P.O. Box 20516, 05508 São Paulo, São Paulo, Brazil
(Received 19 September 1985)

The Compton profiles of W, Ag, and Cu were measured for three scattering angles (30°, 15°, and 10°) using ^{137}Cs γ rays. A Monte Carlo simulation was used to reproduce the experimental situation. Double-scattering events are considered in the simulation and subtracted from the single profile when necessary. Good accordance with the theoretical momentum distribution of the electron cloud was observed when relativistic wave functions quoted by Mendelsohn, Biggs, and Mann are used. This accordance was achieved only when the Ribb ers correction of the Compton profile was considered.

I. INTRODUCTION

It is known that measurements of the Compton profile can provide information about the projection of electronic momentum distribution on the scattering wave vector. The interpretation of experimental results requires the knowledge of the wave functions of all electrons of the atom so that the Compton profile can serve as an excellent test for wave functions obtained from different models.

Most measurements of the Compton profile were done at scattering angles close to 180°, since the impulse approximation (Ribberfors[1,2]) implies a differential cross section (in the nonrelativistic region) simply proportional to the Compton profile,

$$J(p_z)=\int dp_x \int dp_y \rho(\mathbf{p}) .$$

Here $\rho(\mathbf{p})$ is the momentum distribution of the electron system before scattering and p_z is the component of the electron momentum along the scattering vector.

Ribberfors showed that the Compton profile can be defined at all scattering angles. It is possible to calculate the Compton profile at any scattering angle $J_{0^\circ}(p_z)$ from the knowledge of the Compton profile at $\theta=180°$, $J_{180^\circ}(p_z)$, providing we multiply the value calculated at 180° by the factor $f(p_z)$ defined by Ribberfors[1,2] as

$$f(p_z)=\frac{X_{180^\circ}}{\tilde{X}[1+p_z(\omega-\omega')/m\,|\mathbf{k}-\mathbf{k}'|]} , \quad (1)$$

where $\mathbf{k}$ and $\mathbf{k}'$ are the wave vectors of the incident and scattered photons, X_{180° and $\tilde{X}$ are factors already defined by Ribberfors and w and w' the energies of the incident and scattered photons.

We decided to make measurements at scattering angles different from 180° in order to verify Ribberfors's considerations. Obviously this is based on the principle that there are "good" wave functions to describe atomic electrons. In this work we assume that the relativistic Hartree-Fock wave functions developed by Mendelsohn, Biggs, and Mann[3] are sufficiently accurate.

There are essentially two advantages in measuring the Compton profile at scattering angles differing from 180°. One of them is just experimental and is connected with the intensity of Compton scattering, since the cross section is larger at small angles. The order is connected with an easier interpretation of data, because in the case of small scattering angles the γ's from multiple scattering will be spread over a larger energy region and this will affect much less the single Compton profile.

II. EXPERIMENTAL TECHNIQUES AND DATA PROCESSING

The main features of the experimental technique have been described previously (Heller and Moreira[4]). A Compton profile measurement was made at room temperature, using 662-keV γ rays of ^{137}Cs, scattered from the sample through angles of 30.1°±0.7°, 15.0°±0.4°, and 10.9°±0.3°.

The apparatus is similar to that previously described (Heller and Moreira[4]). The intensity of the source was 30 Ci. The targets were plates of W, Ag, and Cu with the dimensions shown in Table I.

Systematic measurements of the three elements in reasonable time spans (a few hours) were performed. A typical spectrum is shown in Fig. 1. The spectra were corrected by subtracting the background and taking into account the detector efficiency; then they are fitted to a function that is the sum of a Lorentz and Gaussian function plus a straight line.

In Table II we present the best fits to the experimental data for the three elements; for one of the elements we have spectra for two different sample thicknesses (the sample thickness is listed in Table I and double thickness is twice that). The figures quoted under the χ^2 column

TABLE I. Dimensions of the samples.

Element	Width (mm)	Length (mm)	Thickness (mm)
W	16.5	61.0	0.8
Ag	20.0	50.0	2.0
Cu	22.0	61.0	6.0

TABLE II. Comparison of experimental and theoretical results for the three scattering angles (30.1°, 15.0°, and 10.9°) for the five elements studied.

Angle	Element	Thickness	$\epsilon_{1/2}$ (keV) Experimental	χ^2	$\epsilon_{1/2}$ (keV) Theoretical	χ^2
30.1°	Pb	Single	14.21±0.95	0.952	15.00±1.04	1.240
		Double	14.16±0.89	1.130		
	W	Single	13.62±0.81	1.093	14.00±0.98	1.240
	Ag	Single	12.28±0.74	0.977	12.97±0.89	1.132
		Double	12.13±0.72	0.987		
	Cu	Single	12.56±0.75	1.120	12.79±0.87	1.167
	Al	Single	10.53±0.63	1.470	10.87±0.75	1.960
15.0°	Pb	Single	8.58±0.51	1.002	9.24±0.64	1.480
		Double	9.24±0.55	1.423		
	W	Single	9.20±0.55	1.062	9.64±0.66	1.147
	Ag	Single	7.38±0.44	0.973	7.52±0.52	0.930
	Cu	Single	7.58±0.45	1.231	7.50±0.55	1.077
	Al	Single	6.40±0.38	0.978	7.06±0.49	1.010
10.9°	Pb	Single	9.00±0.54	1.110	8.10±0.56	1.180
		Double	8.00±0.48	1.190		
	W	Single	8.52±0.51	1.044	7.87±0.54	1.190
	Ag	Single	7.55±0.45	1.000	7.00±0.48	0.930
		Double	6.41±0.41	1.020		
	Cu	Single	7.29±0.43	1.257	6.60±0.46	1.520
	Al	Single	6.54±0.39	1.346	6.53±0.45	0.824

are the χ^2 per degree of freedom. We noted that in the cases of single and double thickness ($\epsilon_{1/2}$) the full width at half maximum (FWHM) did not show remarkable variations that could be attributed to double scattering. However, at low energy far from the Compton peak, the counting rate, although small (factor $\frac{1}{100}$ in relation to peak) was not zero due to double scattering.

To make a comparison of our experimental results with theoretical predictions we constructed the spectral distribution of scattered γ's using the electronic wave functions, as described in detail in Ref. 4.

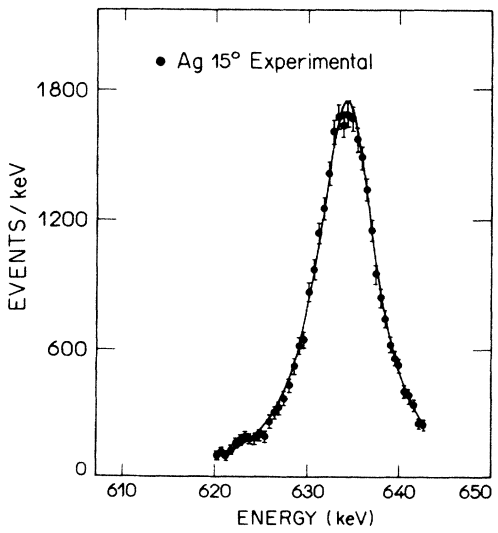

FIG. 1. Scattered photon energy distribution for Ag at 15°, experimental results.

III. ANALYSIS

From the computational simulation it was possible to construct the energy spectrum of the scattered γ. Table III gives the FWHM of the simulated spectra for the three elements calculated at 30° for the case of a realistic simulation (orbital electrons in motion) and for an ideal situation of electrons at rest. We clearly see the broadening in the spectra caused by the movement of the electrons, which decreases with the decreasing scattering angle, but is still adequate to give information on the electronic momentum distribution at angles larger than 10°.

To reproduce the experimental spectra from calculations we must consider the double scattering contribution. We find that the total number of double events in the region of interest is $\simeq 2\%$ for W and $\simeq 1\%$ for Ag and Cu, and the double scattering spectrum is reasonably approxi-

TABLE III. FWHM of the energy distribution for the three elements at $\theta = 30°$, under the same geometry for $p_z \neq 0$ and $p_z = 0$. (p_z is the component of the electron momentum, along the scattering vector.)

Element	$\epsilon_{1/2}$ (keV) $p_z \neq 0$	$\epsilon_{1/2}$ (keV) $p_z = 0$
W	15.38±1.06	8.71±0.58
Ag	12.97±0.89	8.00±0.53
Cu	12.79±0.87	8.00±0.53

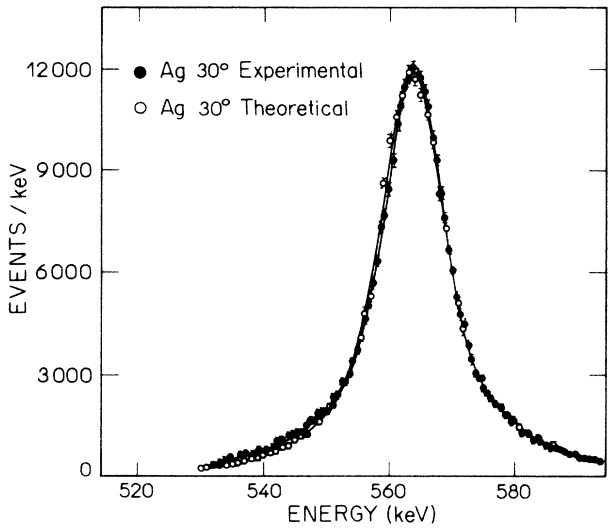

FIG. 2. Scattered photon energy distribution for Ag at 30°, experimental and theoretical results.

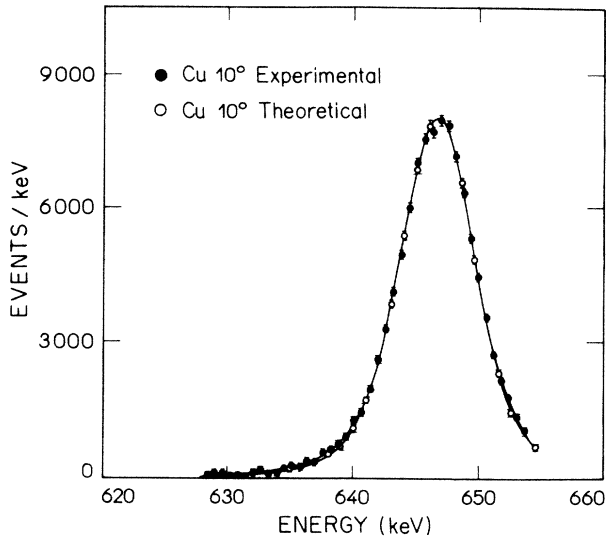

FIG. 4. Scattered photon energy distribution for Cu at 10°, experimental and theoretical results.

mated by a straight line associated to the straight line used for the correction of detector's efficiency.

Figures 2, 3, and 4 show some of the experimental results obtained with background subtraction and correction for detector efficiency. We also display the spectra obtained by computational simulation.

Table II shows the theoretical and experimental data, with the values of $\epsilon_{1/2}$ obtained from the fitting of the analytic functions (Gaussian plus Lorentzian functions) to the Compton measured spectra, and also to the points obtained from the histograms of computational simulation. Figures 5 and 6 provide a simple view of the motion of the electrons since the Compton spectrum FWHM is an increasing function of the atomic number. Even at a very small scattering angle such as 15°, this effect is still noticeable and useful for investigation.

In this table we included results for Pb and Al from Ref. 4. Observing the χ^2 results for the whole set of scatterers and angles we conclude that the analytical functions reproduce quite well the experimental points and the theoretical model. The values of $\epsilon_{1/2}$ listed are obtained measuring the FWHM. The only large χ^2 value is observed for Al at 30° and 10° but as already stated in Ref. 4 no systematic behavior can be deduced from these results.

It should be useful to investigate the sensitivity of our calculation to different electron wave functions. It is also important to discuss the neglect of molecular effects on our metallic targets.

These two issues are discussed in Ref. 4, and in this paper some more analysis is presented concerning the first effect for copper. Figure 7 shows an expanded view of the low-energy tail simulated in our computer model for two different Compton profiles. We compare results

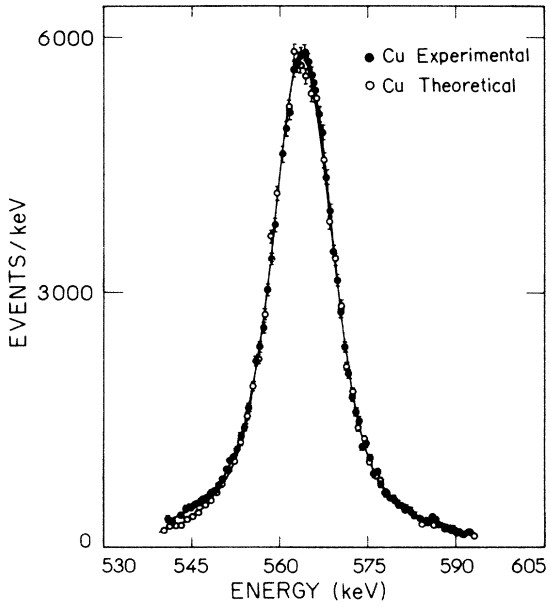

FIG. 3. Scattered photon energy distribution for Cu at 30°, experimental and theoretical results.

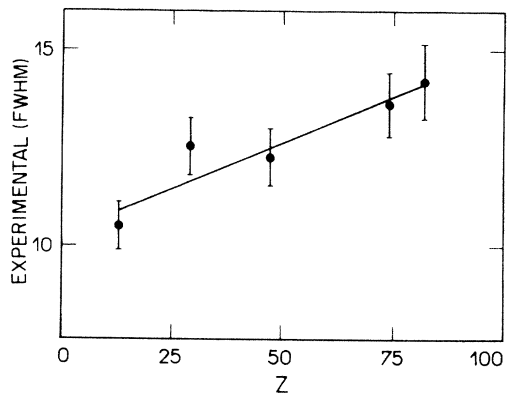

FIG. 5. Experimental FWHM for the five elements at 30°, as a function of atomic number.

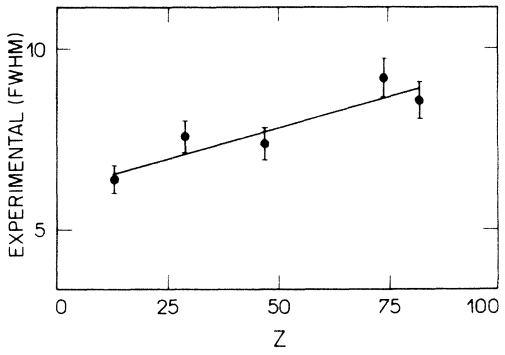

FIG. 6. Experimental FWHM for the five elements at 15°, as a function of atomic number.

yielded from the data of Mendelsohn, Biggs, and Mann[3] with results derived from a modified profile when the K electrons are excluded and all others are unchanged. Figure 8 shows both expanded tails for the Compton scattering spectrum of Cu at 30° simulated using the computer for two different Compton profiles. The narrow profile was calculated using the Mendelsohn *et al.*[3] theoretical data and the other resulted from a modification only in the K shell, where the Mendelsohn[3] data were increased by 50% for p_z ranging from 1 to 5 a.u. and 100% from p_z larger than 5 a.u. [Obviously the new profile was renormalized to ensure that $2\int_0^\infty J(p_z)dp_z=1$ per electron.] Figure 9 shows the investigation of the contribution of the L_{II} shell. The Cu spectra at 30° are evaluated from the Mendelsohn *et al.*[3] profile and from another profile obtained from the previous one by increasing the L_{II} values by 50% for p_z between 1 and 5 a.u. and 100% for other larger values, after renormalization.

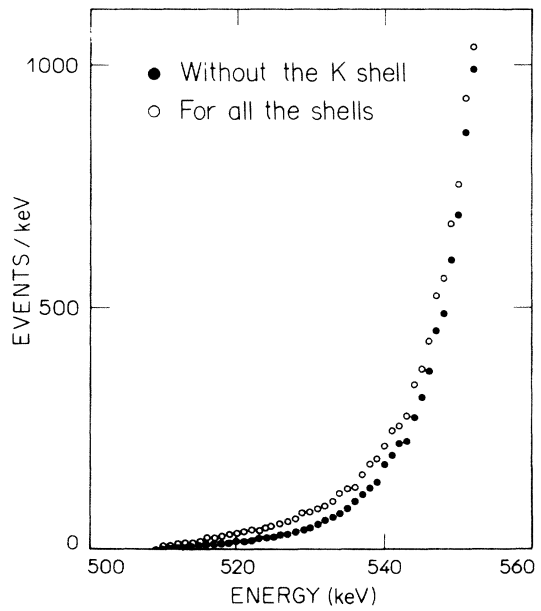

FIG. 7. Expanded view of the low-energy tail for Cu 30°, with and without K shell.

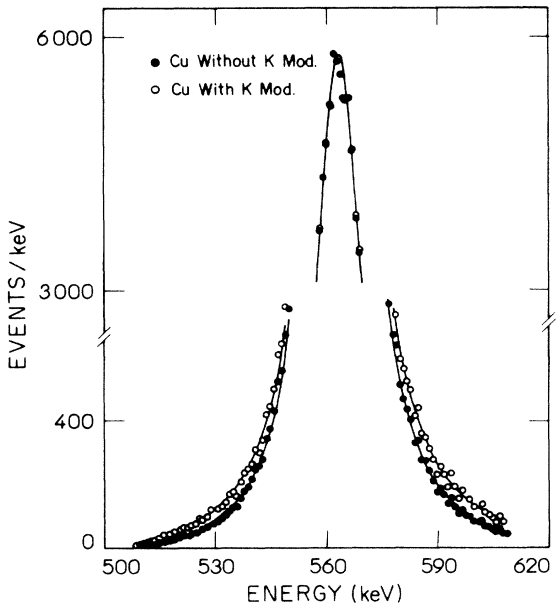

FIG. 8. Cu 30°, with and without K shell modification expanded view of both tails.

IV. CONCLUSION

Our work shows that it is possible to reproduce the experimental results through a computational simulation using Ribberfors[1,2] expression for angles different from 180° and for heavy, medium, and light atoms. The noninclusion of this correction gives rise to a systematic discrepancy discernible in all spectra. Table IV shows the difference in $\epsilon_{1/2}$ for spectra simulated with and without Ribberfors[1,2] correction for Pb, Ag, and Cu at 30°.

The spectra simulated from different Compton profiles for K and L Cu electron shells provide evidence of the

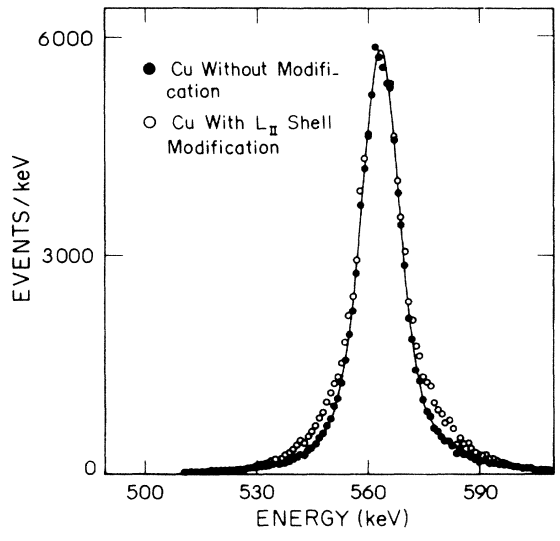

FIG. 9. Cu 30°, with and without L_{II} shell modification.

TABLE IV. Comparison of the Compton profile with and without Ribberfors's correction for Pb, Ag, and Cu. Energy of the incident photon is 662 keV.

Angle	Element	$\epsilon_{1/2}(B)$[a]	$\epsilon_{1/2}(R)$[b]	$\epsilon_{1/2}$(expt)[c]
30°	Pb	13.27±0.50	15.00±1.04	14.21±0.95
30°	Ag	10.90±0.73	12.97±0.89	12.28±0.74
30°	Cu	11.45±0.76	12.79±0.87	12.56±0.75

[a] $\epsilon_{1/2}(B)$ is FWHM distribution without Ribberfors's correction.
[b] $\epsilon_{1/2}(R)$ is FWHM distribution with Ribberfors's correction.
[c] $\epsilon_{1/2}$(expt) is the FWHM of the experimental distribution.

sensitivity of our measurement for identifying good wave functions. Figure 8 shows that a simple scattering measurement carried out in a few hours with our experimental set up is good enough to distinguish a 50—100% change of the K shell, leaving all the other 27 electrons unchanged. Figure 9 allows us to easily detect a 50—100% change in the L_{II} (six electrons) profile. It is clear that a 10% change in this last profile would also be visible in our experimental result. The situation is somewhat more cumbersome for heavy nuclei since the contributions of the K or L shells are much more depressed when compared to the total profile and to the background caused mostly by double scattering, as discussed in Ref. 4 for Pb. In any case it is important to notice that with such simple experimental apparatus it is possible to observe small deviations of the Compton profile with the measurements of Compton spectrum in a reasonable time span (24—48 h).

Further investigation of the "correct" Compton profile could be carried out by trial and error searching for better reproduction of the experimental spectrum. This was not our preliminary objective in this experiment, since our statistics are poor and much better experimental spectra would be desirable before engaging in such an effort.

ACKNOWLEDGMENTS

We are deeply indebted to Professor Max Cohenca and Professor Philippe Gouffon of the Physics Institute of the University of São Paulo for helpful collaboration in all aspects of the computations. The authors are grateful to Professor Marcos Martins for useful comments on the manuscript.

[1] R. Ribberfors, Phys. Rev. B **12**, 2076 (1975).
[2] R. Ribberfors, Phys. Rev. B **12**, 3136 (1975).
[3] L. B. Mendelsohn, F. Biggs, and J. B. Mann, At. Data Nucl. Data Tables **16**, 202 (1975).
[4] M. V. Heller and J. R. Moreira, Phys. Rev. B **31**, 4146 (1975).